Deployment of stent-grafts in curved aneurysmal arteries: towards a predictive numerical tool

David Perrin, Nicolas Demanget, Pierre Badel, Stéphane Avril, Laurent Orgéas, Christian Geindreau, Jean-Noël Albertini

HAL Id: hal-01139049
https://hal.archives-ouvertes.fr/hal-01139049

Submitted on 3 Apr 2015

Deployment of stent-grafts in curved aneurysmal arteries: towards a predictive numerical tool

Perrin D.[1,2,3], Demanget N.[1,2,3], Badel P.[1], Avril S.[1], Orgéas L.[2,3], Geindreau C.[2,3], Albertini J.N.[4]

[1] Ecole Nationale Supérieure des Mines de Saint-Etienne, CIS-EMSE, CNRS:UMR5307, LGF, F-42023 Saint Etienne, France

[2] CNRS, 3SR Lab, F-38000 Grenoble, France

[3] Univ. Grenoble Alpes, 3SR Lab, F-38000 Grenoble, France

[4] CHU Hôpital Nord Saint-Etienne, Department of CardioVascular Surgery, Saint-Etienne F-42055, France.

Corresponding author:

Pierre Badel

Center for Health Engineering, Ecole Nationale Supérieure des Mines

158 cours Fauriel, 42023 SAINT-ETIENNE CEDEX 2 France

Phone: +33477420260, Fax: +33477499755

Email: badel@emse.fr

Document type: Original article

Short title: Deployment of stent-grafts in curved aneurysms

Abstract

The mechanical behavior of aortic stent-grafts plays an important role in the success of endovascular surgery for aneurysms. In this study, finite element analysis was carried out to simulate the expansion of five marketed stent-graft iliac limbs and to evaluate quantitatively their mechanical performances.

The deployment was modeled in a simplified manner according to the following steps: stent-graft crimping and insertion in the delivery sheath, removal of the sheath and stent-graft deployment in the aneurysm, application of arterial pressure.

In the most curved aneurysm and for some devices, a decrease of stent-graft cross-sectional area up to 57% was found at the location of some kinks. Apposition defects onto the arterial wall were also clearly evidenced and quantified. Aneurysm inner curve presented significantly more apposition defects than outer curve.

The feasibility of finite element analysis to simulate deployment of marketed stent-grafts in curved aneurysm models was demonstrated. The influence of aneurysm tortuosity on stent-graft mechanical behavior shows that increasing vessel curvature leads to stent-graft kinks and inadequate apposition against the arterial wall. Such simulation approach opens a very promising way towards surgical planning tools able to predict intra and/or post-operative short-term stent-graft complications.

Introduction

Endovascular aneurysm repair (EVAR) is a widely and increasingly used technique to treat abdominal aortic and iliac aneurysms. However, to date, the main issue of EVAR remains stent-grafts (SG) durability. Secondary interventions after 5 years are required in up to 22% of abdominal aortic aneurysms due to endoleaks, stenosis or thrombosis of the SG, and failure of the SG components [1]–[6]. Despite much more limited number of reports, complications following endovascular repair of iliac aneurysms are similar [7], [8]. In tortuous aneurysms, a lack of SG flexibility has been associated with the above-mentioned complications [9], [10]. These facts clearly emphasize the serious need to better understand and model the mechanical behavior of SGs. In particular, finite element (FE) analyses could be used to predict the deployment of stent-grafts in aneurysm models.

In the literature, many reports have focused on the expansion of stents without any textile [11]–[17]. And yet, the presence of the textile component onto which stents are sutured is a key aspect which drastically influences the device behavior and requires specific modeling. Simplified homogenous stent-graft models with equivalent material combining stent and graft have been used in computational fluid dynamics (CFD) and fluid structure interaction (FSI) studies [18]–[23]. These homogenous models did not take into account the mechanical interactions between stents and graft. Tubular SG models combining nitinol stents and ePTFE fabric have been developed by several groups [24], [25]. However, these models did not reproduce specifically any available marketed SG. Vad et al.[26], focusing on pullout forces, presented simulations of three marketed SG deployed in polymer tubes. De Bock et al. reported the first simulation of a bifurcated marketed SG (Talent, Medtronic) deployed in a silicone mock aneurysm [27], and compression tests on marketed SG [28]. Auricchio et al. performed deployment simulation of a custom made tube endograft in a patient specific CT reconstructed ascending aorta [29]. Our group recently published simulations of eight marketed iliac limbs [30]. Additional fabric traction and bending tests were included in order to refine the mechanical behavior of graft FE model. This study emphasized the role of stent design in the SG mechanical behavior during bending tests.

Towards clinically-relevant simulation, the next step is to address the deployment of realistic stent-graft models in realistic geometries. The goal of the present study was to simulate the expansion of five marketed SG limbs in iliac aneurysms. SGs were deployed in two idealized curved vessels to investigate the effect of vessel tortuosity on SG mechanical response. Hence, in a similar aneurysmal configuration, different SG mechanical behaviors were observed by measuring deployed SG cross section and wall apposition.

Materials and methods

1. Geometry, mesh and constitutive properties of stent-grafts and aneurysms

Limbs of five commercial SGs were modeled:

- Zenith Flex (Ze) (Cook Medical Europe, Bjaeverskov, Denmark),

- Talent (Ta) (Medtronic, Santa Rosa, USA),

- Endurant (En) (Medtronic, Santa Rosa, USA),

- Zenith Low Profile (Zlp) (Cook Medical Europe, Bjaeverskov, Denmark),

- Zenith Spiral Z (Zs) (Cook Medical Europe, Bjaeverskov, Denmark).

Characteristics of limb fabric and stents are depicted in Table 1. Zs SG featured a 316L stainless steel Z-stent at both extremities and a spiral-Z Nitinol stent in between. Fabric was made of polyethylene terephtalate in all SGs. In order to simplify simulations and make relevant comparisons, diameters at proximal and distal ends were identical.

Detailed modeling strategy can be found in a previous study[31]. Briefly, fabric and stents geometries were derived from the manufacturers' specifications and were then respectively discretized with shell and volume finite elements using a custom routine of Matlab® software. Superelastic properties of Nitinol stents were taken from the literature[24] and described with Auricchio's model[32], taking into account the tension-compression asymmetry. The same constitutive parameters as in[31] were used in the present study. Ze and Zs contained 316L stainless steel stents, the elasto-plastic properties of which are reported in[31]. A preliminary mesh convergence analysis has been undertaken to ensure accurate results and get fast computation.

Given literature lack of data on fabric mechanical properties, characterization and modeling of the in-plane and bending behavior was performed. Several uniaxial and plane strain tensile tests were performed on the available fabric samples to provide the Young and shear moduli and Poisson's ratio. In addition, "nail tests" (bending of a fabric strip under its own weight) were used to estimate the longitudinal D_L and transverse D_T bending stiffnesses of the fabric. Detailed description of fabric testing is described elsewhere [31]. We show in Fig. 1 an illustration of the influence of these properties on a pure bending test of the Ze stent-graft, and refer the reader to a previous study[33] for a thorough validation of this model including the essential aspect of fabric modeling.

Two idealized geometries of curved iliac aneurysms, inspired from clinical cases, were designed with CAD software Rhinoceros (McNeel & associates, Seatlle, WA, USA). Aneurysm 1 had a relatively straight anatomy with an angulation between centerlines at proximal and distal ends of 60° (Fig. 2A). Aneurysm 2 featured more pronounced tortuosity with an angulation between centerlines at proximal and distal ends of 180° (Fig. 2B). Intraluminal vessel diameter at both proximal and distal necks was13.3 mm. Wall thickness was 2 mm [34], giving a mean diameter of 15.3 mm. These vessels and SG diameters were

consistent with manufacturers' instructions for use (Table 1). Proximal and distal neck lengths were 38 mm in both aneurysms. Aneurysm 1 and 2 maximum transverse diameters were 30 and 31.2 mm, respectively. The vessel wall was meshed in FE software Abaqus® and was affected the constitutive parameters of a Mooney-Rivlin hyperelastic model reported by Raghavan et al [35].

Friction between the SG and the arterial wall was modeled using the standard Coulomb friction law with a friction coefficient value of 0.2, in the mid-range of experimental values reported in [26] (note that a sensitivity analysis proved that friction coefficient value had negligible influence on the results).

2. Deployment simulation strategy

This section describes the simulation procedure used to compute the positioning of stent-grafts in the given geometries. The insertion of the delivery system and its influence were not considered in this simplified deployment procedure, inspired from [11], that was used to deploy the SGs inside the arteries (Fig. 2C). As in [31], the whole numerical resolution was performed using the explicit solver of Abaqus®, due to severe non-linearities in these simulations (graft wrinkles, contacts). The simulation time and parameters were adjusted to maintain a quasi-static process.

Steps 1 and 2

The first two steps consisted in the insertion of the SG crimped in a delivery sheath inside the aneurysm. For this purpose, the SG was surrounded by a cylindrical tube simulating the delivery sheath. This tube had an initial diameter of 20 mm. Then, the sheath diameter was reduced from 20 to 12 mm and its axis was curved along the aneurysm centerline, allowing both sheath and SG to fit inside the aneurysm. The actual sheath diameters are about 6 mm, however, a preliminary study showed that reducing the sheath diameter to less than 12 mm had no impact on the results.

SGs were longitudinally positioned so that the proximal and distal aneurysm necks were covered by two stents.

Step 3

The third step consisted in removing the delivery sheath to deploy the device. During this step, contact between the SG and the vessel wall was activated while the sheath was progressively removed by increasing its diameter.

Step 4

The SG inner surface was finally subjected to 100 mmHg pressure, average value of diastolic and systolic pressures.

3. Assessment of SG deployment quality

SG deployment in aneurysms 1 and 2 was qualitatively assessed on the basis of visible kinks and arterial wall apposition defects.

5

The following quantitative criteria were also assessed and compared for each SG after deployment in aneurysms 1 and 2.

a. Maximum reduction of SG cross-sectional area ($CSAR_{max}$)
Quantitative assessment of SG kinks was performed by calculating the maximum reduction of SG cross-sectional area ($CSAR_{max}$). A detailed description of this method has been reported in [31]. Areas of cross-sections along the entire SG were measured, before and after deployment in the aneurysm. Before SG deployment, cross-section area was constant along the entire SG and called S_0. Following deployment, cross-sectional areas were reduced, especially at the level of SG kinks. $CSAR_{max}$ was defined as the relative reduction of cross-sectional area between the smallest cross-section of the deployed SG (S_{min}) and the initial cross-section (S_0):

$$CSAR_{max} = 100 \left(1 - \frac{S_{min}}{S_0}\right) (\%)$$

b. Distance between stents and arterial wall (DSA)
Apposition defects were clearly apparent on longitudinal sections of the aneurysm model (Fig 3), where stents and fabric were pulled away from the arterial wall. This aspect was more pronounced for the two most distal stents, in the distal neck of the most tortuous aneurysm 2 (Fig 3B and 3C). As stents have circular topology, two cross-sections per stent could be identified on a longitudinal cross-section view, one along the inner curve, and the other along the outer curve of the aneurysm wall (Fig 3B and 3C). It was then possible to measure the distance d (Fig 3C) and to compute the distance between the stent strut and the arterial wall (DSA) (Fig 3D). Cross sections of the two most distal stents, only, were considered (Fig 3C).
In order to increase the number of DSA measurements, seven consecutive longitudinal sections (± 3 mm from the central section, every 1 mm) were studied (Fig 3A). Therefore a total of 28 DSA measurements were performed for each SG deployed in one aneurysm model.

4. Statistical analysis

Non-parametric tests were used to compare DSA estimates. P-value of 0.05 was considered as a level of statistical significance.

Results

The simulations were run on a 12-core computer (2.6 GHz, 4 Go RAM). Mean CPU time was 42 hours (3:30 real time).

1. Qualitative analysis

Deployed SGs within aneurysms 1 and 2 at the end of the simulation are shown in Figs. 4A and 4B. There is no visible significant kink for all SGs deployed in aneurysm 1. Conversely, significant kinks are visible at the distal end of the Talent (Ta) and the Zenith Flex (Ze) SGs deployed in aneurysm 2. In aneurysm 1, apposition on the arterial wall within proximal and distal necks is satisfactory for all SGs. In aneurysm 2, inadequate apposition of the two most

6

distal stents at the inner curvature is seen for all SGs. At this location, the most distal stent is no longer parallel to the arterial wall.

2. Maximum reduction of SG cross-sectional area

$CSAR_{max}$ ranged between 27% for the En and 32% for the Ta in aneurysm 1. $CSAR_{max}$ ranged between 33% for the En and 57% for the Ta in aneurysm 2 (Fig. 5).

3. Distance between stents and arterial wall

DSA in aneurysms 1 and 2 are depicted in Tables 2A and 2B.

First, the analysis of these results revealed that the SG deployed differently at the inner and outer curvatures. For this reason, DSA measurements were split into two categories: DSAIC and DSAOC, standing respectively for DSA at the inner and outer curvature.

In aneurysm 1, mean DSAOC ranged from 0 mm (En, Ta and Zs) to 0.08 ± 0.15 mm (Ze), with a maximum value of 0.44 mm, and mean DSAIC ranged from 0 mm (En) to 0.06 ± 0.12 mm (Ze), with a maximum value of 0.3 mm. In aneurysm 2, mean DSAOC ranged from 0 mm (En and Zlp) to 0.22 ± 0.29 mm (Ta), with a maximum value of 0.85 mm, and DSAIC ranged from 0.24 ± 0.26 mm (Zs) to 1.22 ± 1.02 mm (Ze), with a maximum value of 3.72 mm (Ta). For all SGs in both aneurysms, DSAIC were greater than DSAOC ($P < 0.01$, Mann-Whitney test), confirming that larger gaps are more likely at the inner curvature.

Second, the selected SG could also be compared based on these results. DSAIC in aneurysm 2 were significantly greater for the Ta and the Ze, compared to the other devices ($P = 0.02$, Kruskall-Wallis test). DSAIC in aneurysm 2 were significantly lower with the Zs, compared to the Ta and the Ze ($P < 0.01$ and $P = 0.01$, respectively; Mann-Whitney Test). The difference was not significant when Zs DSAIC was compared to Zlp DSAIC and En DSAIC.

Discussion

This study has confirmed the feasibility of FE simulation of SG deployment in aneurysm models featuring realistic geometries. The originality of this work is that several marketed SGs were deployed in two aneurysm models presenting different degrees of tortuosity. Several clinically-relevant aspects could be quantified and showed that such simulation is discriminating and has potential for clinical applications in surgical practice.

The model confirmed that angulated recipient artery may favor SG kinks as well as apposition defects onto the arterial wall. Kinks have been related to SG stenosis and/or thrombosis in several clinical studies [2], [5], [36]. Angulation of proximal and distal aneurysm necks is a well-established predictive factor of adverse events following EVAR, particularly type1 endoleaks [37]. Bench test studies have shown that inadequate SG apposition on the arterial wall was a mechanism for type 1 endoleaks [4], [38]. Therefore, the results of the present simulation are relevant to the above mentioned clinical complications.

The present study suggests that precise and relevant information on SGs behavior deployed within arterial models may be provided by numerical simulation. Notice that SG kinks and

associated cross-sectional reduction in aneurysm 2 have similar characteristics to those described during *ex-vivo* bending tests in previous studies [30], [33]. SG inadequate apposition on the arterial wall is predominant at the inner curve of the tortuous vessel. At the vessel outer curve, forces tend to pull consecutive stents apart, but this displacement is quickly limited by fabric stretching. Therefore, stent application on the arterial wall seems to remain adequate at the outer curve. At the inner vessel curve, increasing angulation brings consecutive stent struts close to each other, up to possible overlapping. At this point, stent overlap is limited by fabric resistance and further load results in radial deformation of the Z-stents at the level of the vessel curvature. Modification of stent design impacts the magnitude of stent displacement relative to the arterial wall during deployment in a curved vessel. The present model confirmed that shorter Z-stents with longer inter-stent spaces, as well as spiral design decreases radial stent deformation at the inner vessel curve, resulting in less displacement relative to the arterial wall. Obviously, the relationship between stent/arterial wall distance and endoleaks is the only clinically-relevant parameter and this should be investigated by implementing computational fluids dynamics into the model.

The present model may have interesting applications in the field of preclinical testing of prototypes and new devices. The advantage of FE analyses is that the possibilities of modeling various SGs and aneurysm configurations are virtually infinite. On the contrary, modeling possibilities in bench test experiments are necessarily restricted by the limited quantity of available prostheses and aneurysm models.

Another major application of such simulations would be patient-specific prediction of EVAR intra and/or post-operative complications. Previous pioneering works have paved the way towards this ultimate goal [22], [27], [29]. A lot of research and development remains to be done before such tools will be available to the clinical physician. We have therefore listed below the main limitations of the present model:

- In the present model, SG behavior during flexion test was validated quantitatively [33]. Validation of deployment in aneurysm models is the subject of ongoing studies requiring intensive computations and gathering of a large amount of clinical data.

- Further refinement in SG simulation would require addition of anchorage systems at the proximal end and better characterization of sutures between textile and stents. Mechanical properties of stents and graft should be determined for every SG model individually.

- All marketed SGs, including bifurcated Z-stents, spiral or ring-based designs (Excluder (Gore Medical), Aorfix® (Lombard Medical), Anaconda® (Vascutek), Ovation® (Trivascular)), should be implemented for a more comprehensive comparison.

- These deployment simulations are simplified as they neglect the insertion and removal of the delivery system which are part of the actual surgical procedure. This would affect, first, the arterial geometry in which the SG is deployed and, second, the final geometry as a new equilibrium is reached after removal of the delivery system.

- Modeling blood flow using fluid-structural interaction simulation would be mandatory to confirm the risk of endoleaks and to assess hemodynamic consequences of kinks.

Several perspectives of this work will be considered within the objective of clinical use of such simulation:

- Next step will consist of using patient-specific aneurysms. For that purpose, vessel geometries could be reconstructed from patient-specific geometries obtained from CT scans [39]. The arterial wall could be modeled including anisotropy and calcifications, and thrombus added [39]. Patient-specific constitutive mechanical properties could also be better characterized using dynamic imaging [40].

- The results should be validated in clinical studies comparing simulated stent-grafts in patient-specific aneurysms with corresponding post-operative CT-scans.

- It is likely that the return to the original arterial tortuosity is hampered by the stiffness of the stent-graft system. Therefore, the final shape of the couple stent-graft/artery depends of the respective stiffness of both components. Similarly, the delivery system –inserted and later removed– is likely to affect the final outcome of the surgery. Simulation of the introduction of delivery sheaths in the arterial vasculature is currently underway in our EVAR simulation program; it requires modelling the various components of delivery sheaths as well as stiff guide-wires. The whole surgical procedure could then be simulated to see the influence of the delivery system on SG deployment[41].

Conclusion

This study confirmed the feasibility of finite element analysis to simulate deployment of marketed stent-grafts in curved aneurysm models. Aneurysm morphology influenced stent-graft mechanical response. Increased tortuosity favored stent-graft kinks and inadequate apposition against the arterial wall. Further refinements and clinical validation of this technology could lead to the advent of surgical planning tools able to predict intra and/or post-operative short-term stent-graft complications, such as kinking or inappropriate apposition.

Conflict of interest

J-N. Albertini is proctor for Cook Medical.

References

[1]   R. W. Chang, P. Goodney, L.-Y. Tucker, S. Okuhn, H. Hua, A. Rhoades, N. Sivamurthy, and B. Hill. Ten-year results of endovascular abdominal aortic aneurysm repair from a large multicenter registry. *Journal of vascular surgery* 2013; 58(2): 324–332.

[2]   F. Cochennec, J. P. Becquemin, P. Desgranges, E. Allaire, H. Kobeiter, and F. Roudot-Thoraval. Limb Graft Occlusion Following EVAR : Clinical Pattern , Outcomes and Predictive Factors of Occurrence. *European Journal of endovascular surgery* 2007; 65: 59–65.

[3]   N. Chakfe, F. Dieval, G. Riepe, D. Mathieu, I. Zbali, F. Thaveau, C. Heintz, J.-G. Kretz, and B. Durand. Influence of the Textile Structure on the Degradation of Explanted Aortic Endoprostheses. *European Journal of endovascular surgery* 2004; 27: 33–41.

[4]   J. N. Albertini, J. Macierewicz, S. W. Yusuf, P. W. Wenham, and B. R. Hopkinson. Pathophysiology of proximal perigraft endoleak following endovascular repair of abdominal aortic aneurysms: a study using a flow model. *European journal of vascular and endovascular surgery* 2001; 22(1): 53–6.

[5]   A. Carroccio, P. L. Faries, N. J. Morrissey, V. Teodorescu, J. Burks, E. C. Gravereaux, L. H. Hollier, and M. L. Marin. Predicting iliac limb occlusions after bifurcated aortic stent grafting: Anatomic and device-related causes. *Journal of Vascular Surgery* 2002; 36(4): 679–684.

[6]   M. A. Bartoli, B. Thevenin, G. Sarlon, R. Giorgi, J. N. Albertini, G. Lerussi, A. Branchereau, and P.-E. Magnan. Secondary procedures after infrarenal abdominal aortic aneurysms endovascular repair with second-generation endografts. *Annals of vascular surgery* 2012; 26(2): 166–74.

[7]   I. F. J. Tielliu, E. L. G. Verhoeven, C. J. Zeebregts, T. R. Prins, B. I. Oranen, and J. J. a M. van den Dungen. Endovascular treatment of iliac artery aneurysms with a tubular stent-graft: mid-term results. *Journal of vascular surgery* 2006; 43(3): 440–5.

[8]   G. Parlani, F. Verzini, P. De Rango, D. Brambilla, C. Coscarella, C. Ferrer, and P. Cao. Long-term results of iliac aneurysm repair with iliac branched endograft: a 5-year experience on 100 consecutive cases. *European journal of vascular and endovascular surgery : the official journal of the European Society for Vascular Surgery* 2012; 43(3): 287–92.

[9]   T. E. trial Participants. Endovascular aneurysm repair versus open repair in patients with abdominal aortic aneurysm (EVAR trial 1): randomised controlled trial. *Lancet* 2005; 365(9478): 2179–86.

[10]   J.-N. Albertini, T. Perdikides, C. Soong, R. Hinchliffe, M. Trojanowska, S. Yusuf, C. Clément, and B. R. Hopkinson. Endovascular repair of abdominal aortic aneurysms in patients with severe angulation of the proximal neck using a flexible stent-graft:

European Multicenter Experience. *Journal of cardiovascular surgery* 2006; 47(3): 245–250.

[11]   F. Auricchio, M. Conti, M. De Beule, G. De Santis, and B. Verhegghe. Carotid artery stenting simulation: from patient-specific images to finite element analysis. *Medical engineering & physics* 2011; 33(3): 281–9.

[12]   P. Mortier, G. A. Holzapfel, M. De Beule, D. Van Loo, Y. Taeymans, P. Segers, P. Verdonck, and B. Verhegghe. A novel simulation strategy for stent insertion and deployment in curved coronary bifurcations: comparison of three drug-eluting stents. *Annals of biomedical engineering* 2010; 38(1): 88–99.

[13]   S. Morlacchi and F. Migliavacca. Modeling Stented Coronary Arteries: Where We are, Where to Go. *Annals of biomedical engineering* 2012; 41(7): 1428–1444.

[14]   F. J. H. Gijsen, F. Migliavacca, S. Schievano, L. Socci, L. Petrini, A. Thury, J. J. Wentzel, A. F. W. van der Steen, P. W. S. Serruys, and G. Dubini. Simulation of stent deployment in a realistic human coronary artery. *Biomedical engineering online* 2008; 7: 23.

[15]   G. A. Holzapfel, M. Stadler, and T. C. Gasser. Changes in the mechanical environment of stenotic arteries during interaction with stents: computational assessment of parametric stent designs. *Journal of biomechanical engineering* 2005; 127(1): 166–80.

[16]   K. Takashima, T. Kitou, K. Mori, and K. Ikeuchi. Simulation and experimental observation of contact conditions between stents and artery models. *Medical engineering & physics* 2007; 29(3): 326–35.

[17]   W. Wu, W.-Q. Wang, D.-Z. Yang, and M. Qi. Stent expansion in curved vessel and their interactions: a finite element analysis. *Journal of biomechanics* 2007; 40(11): 2580–5.

[18]   B. A. Howell, T. Kim, A. Cheer, H. Dwyer, D. Saloner, and T. A. M. Chuter. Computational fluid dynamics within bifurcated abdominal aortic stent-grafts. *Journal of endovascular therapy : an official journal of the International Society of Endovascular Specialists* 2007; 14(2): 138–43.

[19]   C. A. Figueroa, C. A. Taylor, V. Yeh, A. J. Chiou, M. L. Gorrepati, and C. K. Zarins. Preliminary 3D computational analysis of the relationship between aortic displacement force and direction of endograft movement. *Journal of vascular surgery* 2010; 51(6): 1488–97.

[20]   Z. Li and C. Kleinstreuer. Analysis of biomechanical factors affecting stent-graft migration in an abdominal aortic aneurysm model. *Journal of biomechanics* 2006; 39(12): 2264–73.

[21]   D. S. Molony, E. G. Kavanagh, P. Madhavan, M. T. Walsh, and T. M. McGloughlin. A computational study of the magnitude and direction of migration forces in patient-specific abdominal aortic aneurysm stent-grafts. *European journal of vascular and*
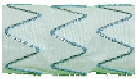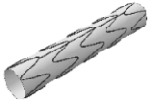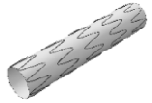
endovascular surgery : the official journal of the European Society for Vascular Surgery 2010; 40(3): 332–9.

[22]   R. Layman, S. Missoum, and J. Vande Geest. Simulation and probabilistic failure prediction of grafts for aortic aneurysm. *Engineering Computations* 2010; 27(1): 84–105.

[23]   S. W. K. Cheng, E. S. K. Lam, G. S. K. Fung, P. Ho, A. C. W. Ting, and K. W. Chow. A computational fluid dynamic study of stent graft remodeling after endovascular repair of thoracic aortic dissections. *Journal of vascular surgery* 2008; 48(2): 303–9.

[24]   C. Kleinstreuer, Z. Li, C. A. Basciano, S. Seelecke, and M. A. Farber. Computational mechanics of Nitinol stent grafts. *Journal of biomechanics* 2008; 41(11): 2370–8.

[25]   A. Prasad, N. Xiao, X.-Y. Gong, C. K. Zarins, and C. A. Figueroa. A computational framework for investigating the positional stability of aortic endografts. *Biomechanics and modeling in mechanobiology* 2012; : 1–19.

[26]   S. Vad, A. Eskinazi, T. Corbett, T. McGloughlin, and J. P. Vande Geest. Determination of coefficient of friction for self-expanding stent-grafts. *Journal of biomechanical engineering* 2010; 132(12): 121007.

[27]   S. De Bock, F. Iannaccone, G. De Santis, M. De Beule, D. Van Loo, D. Devos, F. Vermassen, P. Segers, and B. Verhegghe. Virtual evaluation of stent graft deployment: A validated modeling and simulation study. *Journal of the mechanical behavior of biomedical materials* 2012; 13: 129–39.

[28]   S. De Bock, F. Iannaccone, M. De Beule, D. Van Loo, F. Vermassen, B. Verhegghe, and P. Segers. Filling the void: A coalescent numerical and experimental technique to determine aortic stent graft mechanics. *Journal of biomechanics* 2013; 46(14): 2477–82.

[29]   F. Auricchio, M. Conti, S. Marconi, a Reali, J. L. Tolenaar, and S. Trimarchi. Patient-specific aortic endografting simulation: From diagnosis to prediction. *Computers in biology and medicine* 2013; 43(4): 386–94.

[30]   N. Demanget, A. Duprey, P. Badel, L. Orgéas, S. Avril, C. Geindreau, J.-N. Albertini, and J.-P. Favre. Finite element analysis of the mechanical performances of 8 marketed aortic stent-grafts. *Journal of endovascular therapy : an official journal of the International Society of Endovascular Specialists* 2013; 20(4): 523–35.

[31]   N. Demanget, S. Avril, P. Badel, L. Orgéas, C. Geindreau, J.-N. Albertini, and J.-P. Favre. Computational comparison of the bending behavior of aortic stent-grafts. *Journal of the mechanical behavior of biomedical materials* 2012; 5(1): 272–82.

[32]   F. Auricchio and R. L. Taylor. Shape-memory alloys : modelling and numerical simulations the finite-strain superelastic behavior. *Computer Methods in Applied Mechanics and Engineering* 1997; 143: 175–194.

[33] N. Demanget, P. Latil, L. Orgéas, P. Badel, S. Avril, C. Geindreau, J.-N. Albertini, and J.-P. Favre. Severe Bending of Two Aortic Stent- Grafts: An Experimental and Numerical Mechanical Analysis. *Annals of biomedical engineering* 2012; 40(12): 2674–2686.

[34] M. L. Raghavan, J. Kratzberg, E. Magalha, M. M. Hanaoka, P. Walker, and E. S. Sima. Regional distribution of wall thickness and failure properties of human abdominal aortic aneurysm. *Journal of biomechanics* 2006; 39: 3010–3016.

[35] M. L. Raghavan and D. A. Vorp. Toward a biomechanical tool to evaluate rupture potential of abdominal aortic aneurysm : identification of a finite strain constitutive model and evaluation of its applicability. *Journal of biomechanics* 2000; 33: 475–482.

[36] G. A. J. Fransen, P. Desgranges, R. J. F. Laheij, P. L. Harris, and J.-P. Becquemin. Frequency, predictive factors, and consequences of stent-graft kink following endovascular AAA repair. *Journal of endovascular therapy : an official journal of the International Society of Endovascular Specialists* 2003; 10(5): 913–8.

[37] W. C. Sternbergh, G. Carter, J. W. York, M. Yoselevitz, and S. R. Money. Aortic neck angulation predicts adverse outcome with endovascular abdominal aortic aneurysm repair. *Journal of vascular surgery* 2002; 35(3): 482–6.

[38] J.-N. Albertini, M.-A. DeMasi, J. Macierewicz, R. El Idrissi, B. R. Hopkinson, C. Clément, and A. Branchereau. Aorfix stent graft for abdominal aortic aneurysms reduces the risk of proximal type 1 endoleak in angulated necks: bench-test study. *Vascular* 2005; 13(6): 321–6.

[39] Z.-Y. Li, U. Sadat, J. U-King-Im, T. Y. Tang, D. J. Bowden, P. D. Hayes, and J. H. Gillard. Association between aneurysm shoulder stress and abdominal aortic aneurysm expansion: a longitudinal follow-up study. *Circulation* 2010; 122(18): 1815–22.

[40] A. Franquet, R. Le Riche, P. Badel, F. C. Schneider, Z. Y. Li, C. Boissier, and J. P. Favre. A new method for the in vivo identification of mechanical properties in arteries from cine MRI images : theoretical framework and validation . *IEEE transactions on medical imaging* 2013; 32: 1448–1461.

[41] A. Kaladji, A. Dumenil, M. Castro, A. Cardon, J.-P. Becquemin, B. Bou-Saïd, A. Lucas, and P. Haigron. Prediction of deformations during endovascular aortic aneurysm repair using finite element simulation. *Computerized medical imaging and graphics : the official journal of the Computerized Medical Imaging Society* 2013; 37(2): 142–9.

List of tables

Table 1: Characteristics and dimensions of five marketed iliac limbs

	Endurant	**Talent**	**Zenith Trifab**	**Zenith LP**	**Zenith Spiral Z**
Overview					
CAD model					
Graft diameter (mm)	15.58	15.48	15.70	15.64	15.58
Graft length (mm)	91.5	108.1	99.4	92.9	90.7
Stent height (mm)	8.3	14.6	11.7	8.6	-
Stent material	Nitinol	Nitinol	Stainless steel	Nitinol	Stainless Steel/Nitinol
Stent configuration	Z	Z	Z	Z	Spiral
Recommended vessel diameter (mm)*	12-14**	12-14**	14-15	13-15	14-15

*: Extracted from manufacturers' Instructions For Use

* *: Internal vessel diameter

14

Table 2A. Distances between stent cross section and adjacent arterial wall (DSA) in distal neck of aneurysm 1

Stent-graft	DSA Outer curvature (mm)*	DSA max outer curvature (mm)	DSA inner curvature (mm)*	DSA max inner curvature (mm)
Endurant	0	0	0	0
Talent	0	0	0.06±0.12	0.3
Zenith	0.08±0.15	0.44	0.04±0.09	0.3
Zenith LP	0.03±0.04	0.1	0.006±0.02	0.09
Zenith spiral	0	0	0.03±0.07	0.19

*Estimates are mean±standard deviation

Table 2B. Distances between stent cross-section and adjacent arterial wall (DSA) in distal neck of aneurysm 2

Stent-graft	DSA outer curvature (mm)	DSA max outer curvature (mm)	P value*	DSA inner curvature (mm)	DSA max inner curvature (mm)	P value**
Endurant	0	0	1	0.63±0.58	1.87	**0.0001**
Talent	0.22±0.29	0.85	**0.003**	1.20±1.06	3.72	**0.0001**
Zenith	0.09±0.11	0.4	0.35	1.22±1.02	3.01	**0.001**
Zenith LP	0	0	0,21	0.66±0.7	2.1	**0.001**
Zenith spiral	0.03±0.06	0.18	0.35	0.24±0.26	0.79	**0.01**

Estimates are mean±standard deviation

* Comparison of outer curvature DSA between aneurysm 1 and 2 (Mann-Whitney Test)

** Comparison of inner curvature DSA between aneurysm 1 and 2 (Mann-Whitney Test)

Legends for illustrations

Figure 1: Illustration of the influence of the textile constitutive model on a pure bending test with the Ze stent-graft. At the top, the proper model including orthotropic properties and adjusted bending stiffness. At the bottom, two examples where respectively orthotropy and bending stiffness adjustment are not considered.

Figure 2: SG deployment simulation method. (A and B) Geometry and dimensions (in mm) of the aneurysm models. (C) Scheme of the different steps used to run the FE simulation.

Figure 3: Distance stents/artery (DSA) measurement. Aneurysm was sliced in seven longitudinal sections and corresponding DSA measurements were performed for all sections (A). The two most distal stents were investigated (B). For each longitudinal slice, measurements of the distance d between the stent strut cross-sections and the adjacent arterial wall were performed (C); DSA were finally calculated from d according to (D).

Figure 4: Deployed SGs in aneurysms 1 (A) and 2 (B). Black circles highlight the location of gaps between SG and arterial wall.
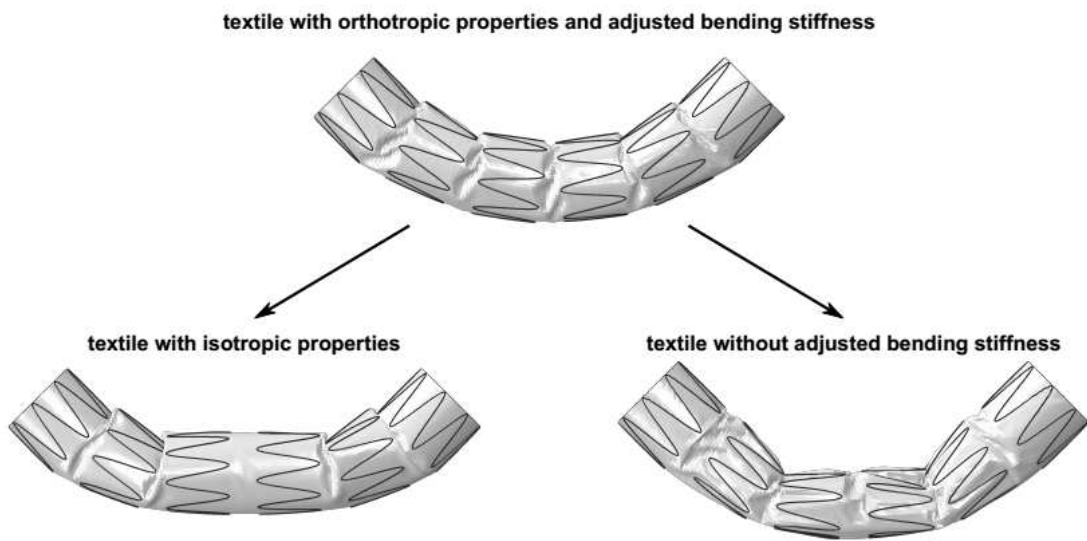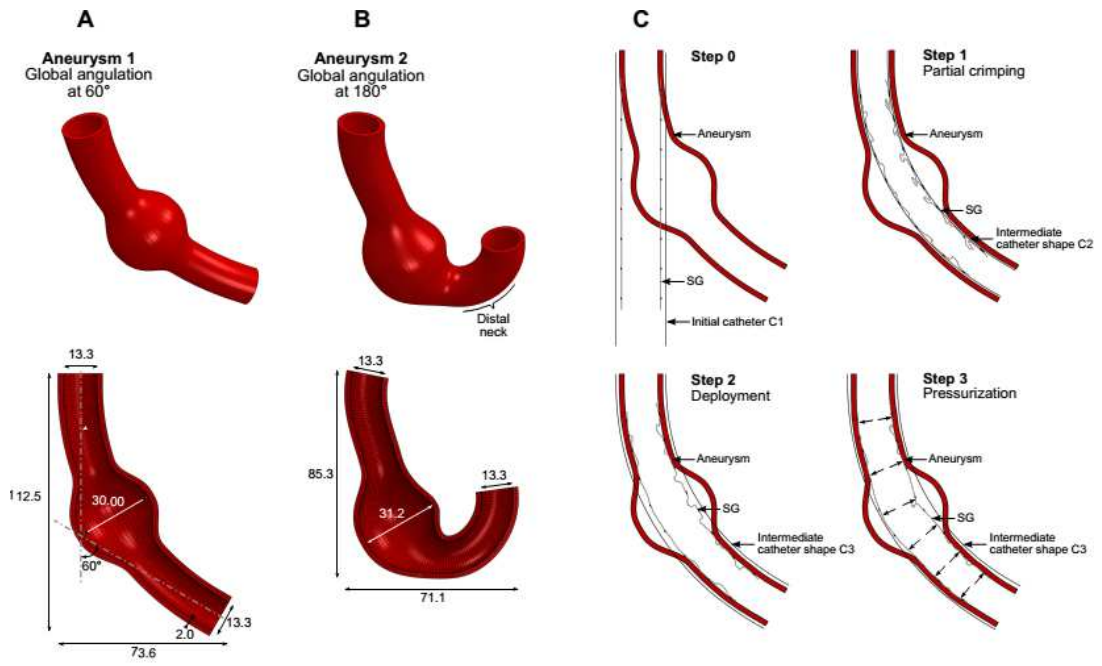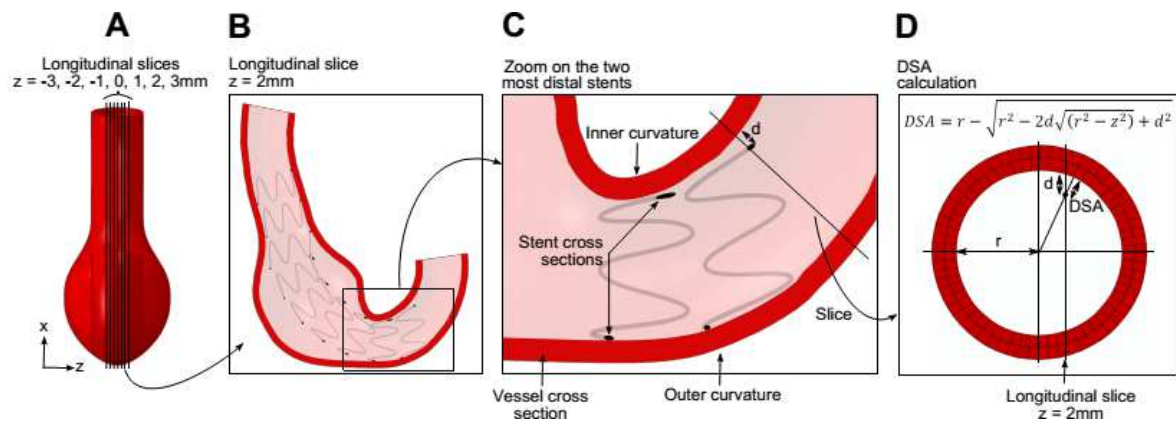
Figure 5: $CSAR_{max}$ in aneurysms 1 and 2

Fig. 1

textile with orthotropic properties and adjusted bending stiffness

textile with isotropic properties

textile without adjusted bending stiffness

Fig. 2

Fig. 3

A Longitudinal slices
z = -3, -2, -1, 0, 1, 2, 3mm

B Longitudinal slice
z = 2mm

C Zoom on the two
most distal stents

Inner curvature

Stent cross
sections

Vessel cross
section

Outer curvature

Slice

d

D DSA
calculation

$$DSA = r - \sqrt{r^2 - 2d\sqrt{(r^2 - z^2)} + d^2}$$

d
DSA
r

Longitudinal slice
z = 2mm

19

Fig. 4

Fig. 5